OXFORD

Sleep Research Society®

ORIGINAL ARTICLE

Cortical autonomic network gray matter and sympathetic nerve activity in obstructive sleep apnea

Keri S. Taylor[1], Philip J. Millar[1,2], Hisayoshi Murai[1], Nobuhiko Haruki[1],
Derek S. Kimmerly[1,3], T. Douglas Bradley[1], and John S. Floras[1,*]

[1]Department of Medicine, University Health Network and Mount Sinai Hospital, University of Toronto, Toronto, Ontario, Canada, [2]Department of Human Health and Nutritional Sciences, University of Guelph, Guelph, Ontario, Canada and [3]School of Health and Human Performance, Faculty of Health Professions, Dalhousie University, Halifax, Nova Scotia, Canada

*Corresponding Author: John S. Floras, 6ES414-200 Elizabeth Street, Toronto, ON M5G 2C4, Canada. Email: john.floras@utoronto.ca.

Abstract

The sympathetic excitation elicited acutely by obstructive apnea during sleep (OSA) carries over into wakefulness. We hypothesized that OSA induces structural changes in the insula and cingulate, key central autonomic network elements with projections to brainstem sympathetic premotor regions. The aims of this study were to (1) apply two distinct but complementary methods (cortical thickness analysis [CTA] and voxel-based morphometry [VBM]) to compare insula and cingulate gray matter thickness in participants without and with OSA; (2) determine whether oxygen desaturation index (ODI) relates to cortical thickness; and (3) determine whether cortical thickness or volume in these regions predicts muscle sympathetic nerve activity (MSNA) burst incidence (BI). Overnight polysomnography, anatomical magnetic resonance imaging, and MSNA data were acquired in 41 participants with no or mild OSA (n = 19; 59 ± 2 years [Mean ± SE]; six females; apnea–hypopnea index [AHI] 7 ± 1 events per hour) or moderate-to-severe OSA (n = 22; 59 ± 2 years; five females; AHI 31 ± 4 events per hour). Between-group CTA analyses identified cortical thinning within the left dorsal posterior insula and thickening within the left mid-cingulate cortex (LMCC), whereas VBM identified thickening within bilateral thalami (all [$p < .05$]). CTA revealed inverse relationships between ODI and bilateral dpIC and left posterior cingulate cortex (LPCC) or precuneus thickness. Positive correlations between BI and LMCC gray matter thickness or volume were evident with both methods and between BI and left posterior thalamus volume using VBM. In OSA, the magnitude of insular thinning, although a function of hypoxia severity, does not influence MSNA, whereas cingulate and thalamic thickening relate directly to the intensity of sympathetic discharge during wakefulness.

Statement of Significance

Sympathetic excitation elicited by obstructive apneas is sustained into wakefulness. Such resetting has been attributed to apnea- or hypoxia-induced functional or structural adaptations in reflex and central pathways generating or modulating sympathetic traffic. Autonomic network morphology characterization by magnetic resonance imaging identified left mid-cingulate and left posterior thalamic thickening in participants with moderate-to-severe obstructive sleep apnea relative to controls; thickness correlated with muscle sympathetic burst incidence. Left insular thickness correlated inversely with oxygen desaturation but was unrelated to sympathetic firing. These observations reveal obstructive apnea-associated cortical structural alterations in regions participating in neural circulatory regulation. The accompanying sympathoexcitation could promote cardiovascular or metabolic pathology. To be determined is the long-term impact of abolishing apnea on these structural and functional maladaptations.

Key words: cortical thickness analysis; intermittent hypoxia; obstructive sleep apnea; sympathetic nervous system; voxel-based morphometry

Introduction

Sympathetic nervous system excitation is intimately linked to the pathophysiology, morbidity, and foreshortened life expectancy of patients with disorders as common and diverse as hypertension, heart failure, arrhythmias, chronic renal injury, and insulin resistance [1–6]. Greater understanding of central neural mechanisms for such activation is fundamental to modifying, beneficially, the clinical trajectory of individuals with these conditions.

One important cause of sympathetic excitation is obstructive sleep apnea (OSA). Obstructive apnea initiates a cascade of mechanical, chemical, alerting, and inflammatory stimuli that elicit acute increases in efferent sympathetic discharge during sleep and induce chronic sustained elevation of the set-point for central sympathetic outflow during wakefulness [7–12]. The latter may result from long-term functional or structural neural adaptations to the recurring sleep-related apnea and hypoxia characteristic of this condition [11].

Using independent component analysis of resting-state brain magnetic resonance (MR) images, we have identified a positive relationship between the strength of functional connectivity within the salience network (SN), a set of brain areas overlapping with the cortical autonomic network (CAN), and multiunit muscle sympathetic nerve activity (MSNA) burst incidence (BI), a direct measure of efferent postganglionic sympathetic activity [13]. The strength of connectivity within the insula, cingulate, thalamus, and cerebellum was greatest in participants with the highest daytime MSNA BI, but independent of the severity of OSA [13]. It is now recognized that the insular and anterior cingulate cortices (ACCs) are anatomically core (but not exclusive) CAN components [14–16] with reciprocal connections with brain stem premotor autonomic neurons that ultimately project to and influence preganglionic sympathetic and parasympathetic outflow [16]. Clinical functional magnetic resonance imaging (MRI) studies of Valsalva's maneuver [17], lower body negative pressure [18], cold pressor test [19], inspiratory capacity apnea [20], Mueller maneuvers, end-expiratory breath holds [21], and task-free conditions [22, 23] have identified these cortices to be premotor autonomic nuclei that respond to salient stimuli with adaptive changes in sympathetic tone [13].

MRI comparing brain structure of individuals with OSA and control participants considered free of sleep-related breathing disorders has identified cortical gray matter volume changes in several regions, including areas that participate in autonomic cardiovascular regulation [22, 24–27]. Voxel-based morphometry (VBM) is used extensively by the neuroimaging community but is subject to errors of misalignment, particularly of the cortex [28, 29]. An alternate method, cortical thickness analysis (CTA), resolves such misalignment and also quantifies data in units of millimeters which are intuitively more comprehensible than gray matter "density" or "volume" quantities generated by VBM. The principal disadvantage of CTA is that it cannot quantify morphology of subcortical brain areas of potential interest, such as the thalamus.

The present analysis, involving participants with and without OSA, confirmed in each by polysomnography, had three objectives. The first was to acquire and compare mean morphometric CTA and VBM data, focusing specifically on previously identified cortical autonomic regions of interest. We hypothesized that the structure of regions participating in the regulation of sympathetic outflow, such as the insula and cingulate [13, 21, 22, 24], would differ between individuals with and without OSA. Because the recurrent hypoxia characteristic of OSA has been identified as a potent stimulus to neural plasticity and increased central sympathetic outflow [11], our second objective was to determine whether the oxygen desaturation index (ODI; the frequency per hour of sleep that blood oxygen saturation dips by 3% or more) relates to the cortical thickness of brain regions involved in autonomic regulation. The third objective was to determine whether MSNA BI relates to the thickness or density of such regions. We hypothesized that significant correlations would be evident between MSNA BI and the thickness or density of regions affected by OSA and involved in the generation or modulation of efferent sympathetic discharge.

Methods

Participants

Healthy individuals were invited primarily by advertisement to participate in this University Health Network Research Ethics Board approved research protocol, involving overnight polysomnography, daytime sympathetic nerve recording, and MR image acquisition. This call for volunteers sought two groups of healthy participants: those who considered themselves likely to have sleep apnea and those who were confident that they did not have sleep apnea. Acknowledging the substantial prevalence of asymptomatic and therefore unrecognized OSA in the general and often nonobese population [30, 31], we chose to categorize participants as having either moderate-to-severe OSA (apnea–hypopnea index [AHI] ≥ 15) or no or mild OSA (AHI < 15) on the basis of polysomnographic evidence. This design contrasts with the common practice of selecting an OSA cohort on the basis of symptom-prompted physician referral for polysomnography (which biases towards the sleepy and obese) and the recruitment for comparison, as control participants, individuals assumed simply by self-report to be free from OSA.

After providing written informed consent, participants completed medical and MRI-readiness questionnaires to ensure eligibility and safe exposure to the magnetic field. Excluded from study were OSA patients being treated with continuous positive airway pressure, current smokers, and individuals with a history or the presence of heart failure, myocardial infarction, predominantly central sleep apnea, refractory hypertension, kidney disease, autonomic neuropathy, neurological impairment, chronic back pain, claustrophobia, imbedded magnetic objects, pregnancy, or Raynaud's phenomenon.

Experimental design

All participants underwent three testing sessions involving (1) overnight polysomnography, (2) daytime microneurographic and physiological recording, and (3) MRI. Microneurographic and MRI sessions were scheduled in random order approximately 1 week apart but on both occasions at the same time of day, 2–3 hr after a similar light meal, and after ≥12 hr of abstinence from caffeine or alcohol. Participants voided before starting each test session.

Polysomnography

To assess self-reported daytime sleepiness, the Epworth Sleepiness Scale questionnaire [32] was administered before

instrumentation by a trained technician unaware of this study's purpose. Sleep stages and arousals from sleep were identified by standard recording techniques and analytical criteria [33–36]. Thoraco-abdominal movements and tidal volume were measured by respiratory inductance plethysmography [35]. Airflow was measured by nasal pressure cannulae [35] and arterial oxyhemoglobin saturation (SaO2) by oximetry. The ODI was calculated for each participant as the frequency, per hour of sleep, that blood oxygen saturation dipped by 3%, or more, from baseline. Based on their AHI, participants were categorized as having no (<5 events per hour), mild (5–15 events per hour), or moderate-to-severe (≥15 events per hour) OSA [35, 36]. At the initiation of this research protocol, the sleep laboratory did not incorporate ODI data routinely into its standard polysomnographic report. Consequently, ODI data are unavailable for the first four of the participants identified as having no or mild OSA and from the first study participant with moderate-to-severe OSA. ODI is the only variable presented for which the data set is incomplete.

Sympathetic nerve recordings

These and related physiological data were acquired in a quiet, temperature-controlled room with participants lying supine, with eyes closed but awake, and breathing spontaneously. Heart rate (HR) was derived from Lead II of an electrocardiogram. Arterial blood pressure was recorded continuously and noninvasively by photoelectric plethysmography (Portapres Model-2, FMS, Finapres Medical Systems BV, Amsterdam, The Netherlands). Each minute, these measurements were referenced to noninvasive oscillometric determinations of brachial artery blood pressure acquired from the opposite arm using a standard 23–33 cm adult cuff (Dinamap Pro 100, Critikon, Tampa, FL, USA). Respiration was recorded using a pneumobelt connected to a pressure transducer. Multiunit postganglionic MSNA was recorded using a unipolar tungsten microelectrode inserted percutaneously into a fascicle of the right common fibular nerve according to previously published methods [37, 38]. Spontaneous discharge was considered to arise from a postganglionic muscle sympathetic fascicle and accepted for analysis if it fired in a fixed temporal relationship to the preceding R wave of the electrocardiogram, was not elicited by skin stroking or an arousal stimulus, increased in frequency or amplitude in response to voluntary apnea, and exhibited a signal-to-noise ratio of ≥3:1. MSNA, blood pressure, and HR were acquired during spontaneous breathing over 10 min of rest. Signals underwent analog-to-digital conversion for storage on a standard PC desktop and subsequent analysis using the LabVIEW software platform (National Instruments, Austin, TX, USA). To address between-participant variation in HR, MSNA was expressed as the conventional cardiac frequency-independent measure of central sympathetic outflow, bursts per 100 heart beats or BI.

MR images

Data were acquired with participants supine within a 3T GE (HDxt 16.0) MRI system fitted with an eight-channel–phased array head coil. A three-dimensional high resolution anatomical scan of the whole brain (120 slices, 24 × 24 cm FOV, 256 × 256 matrix, 1.5 × 0.859 × 0.859 voxels) was acquired with a T1-weighted 3D spoiled gradient echo sequence (flip angle = 45°, TE = 5 ms, TR = 25 ms).

Cortical thickness analysis

CTA was performed using freesurfer (http://freesurfer.net/) as described in detail [39–42]. Briefly, each participant's T_1-weighted high resolution scan was first registered to the Talairach atlas [43]. This was followed by intensity normalization, skull stripping, and separation of the hemispheres. The border between the gray/cerebrospinal fluid (CSF) (pial surface) and white/gray matter (white surface) was identified, segmented, and the distance between the pial and white surfaces calculated at every point in each hemisphere of the brain. In order to perform group analyses, each hemisphere was inflated into a sphere and iterative alignment algorithms used to align sulci and gyri between participants [39–41]. As there is inherent anatomical heterogeneity between participants, a 10-mm full width half maximum (FWHM) spatial smoothing kernel was applied prior to statistical analysis. General linear model (GLM) analyses (see Statistical Analysis for specific comparisons) were then performed at every point on the brain. To reduce the number of multiple comparisons and focus on our specific hypotheses, this analysis was restricted to the bilateral cingulate and insular cortices by incorporating a mask (taken from Freesurfer's built in atlas) to the GLM. A Monte Carlo simulation, with AlphaSim (implemented within the AFNI software package; http://afni.nimh.nih.gov/afni/), computed the probability of a random field of noise producing a cluster of a given size after thresholding at a given p-value (see also Ref. 44). Data are displayed at a corrected $p < .05$, and derived from an uncorrected $p < .0075$ and 245 contiguous vertices, where the distance between two vertices is 0.80 mm².

Voxel-based morphometry

VBM was implemented in SPM12 (http://www.fil.ion.ucl.ac.uk/spm/) [45]. The origin of each participant's T1-weighted high resolution image was manually set to the anterior commissure. Images were segmented into gray matter, white matter, and cerebral spinal fluid. Segmented images were then registered iteratively using DARTEL (Diffeomorphic Anatomical Registration Through Exponentiated Lie algebra) [46]. This process creates a high resolution template for the group of individuals which is subsequently normalized to MNI stereotactic space using affine and nonlinear spatial normalizations. Each individual participant's native space gray matter images were then registered to the highest resolution gray matter template, resampled to 1.5 mm³ voxel size, modulated to restore volumetric information, and spatially smoothed with a 10-mm FWHM isotropic Gaussian kernel. GLMs were then constructed (see Statistical Analysis for specific comparisons). Total intracranial volume (TICV) was included as a covariate of no interest. GLM analyses were restricted to the thalamus, insula, and cingulate cortices by utilizing a mask (taken from SPM's built in atlas) in the GLM. Specific cortical locations were determined by referencing the peak talairach coordinates to the Talairach atlas [43] and, for more specific thalamic nuclei, using Talairach Client (http://www.talairach.org/client.html). Data are displayed with a family-wise error (FWE) cluster corrected probability, $p < .05$.

Statistical analysis

To determine first the impact of OSA on gray matter thickness, using both CTA and VBM techniques, GLMs were constructed so

as to compare participants with no or mild OSA to those with moderate-to-severe OSA. To delineate the effect of repetitive episodes of nocturnal hypoxia on cortical thickness, a correlation analysis was constructed between ODI and cortical thickness. This GLM included age as a covariate. Finally, to establish whether structural changes were linked to augmented sympathetic outflow, correlation analyses were performed across all participants by regressing gray matter volume or thickness with MSNA BI. Age was included as a covariate. Considering the small absolute number, but similar proportion of women in both groups, to avoid a type II statistical error, we elected not to include sex as a covariate. At the initiation of this research protocol, the sleep laboratory did not incorporate ODI data routinely into its standard polysomnographic report.

Results

Participant characteristics

Of the 30 men and 11 women who completed this protocol, 22 (five women) were determined to have moderate-to-severe OSA (AHI = 31 ± 4 [mean ± SE]). The remaining 19 (six women) with no or mild sleep apnea (AHI = 7 ± 1) were categorized as control (C) participants for the purpose of the present comparison. Participant characteristics are presented in Table 1. As anticipated, mean values for both MSNA BI (71 ± 3 vs. 55 ± 4 bursts/100 heart beats) (p < .001) and ODI (35 ± 2 vs. 10 ± 2 events per hour) were significantly greater in OSA participants (p < .001 for both), whereas the mean Epworth Sleepiness Scale was similar, and in the nonsleepy range. There were no significant differences in MSNA BI between men and women of either group. Handedness was identified in 35 individuals. All 17 with no or mild apnea and 17 of the 18 with moderate or severe OSA were dexterous.

Gray matter thickness

CTA identified a large region situated within the left dorsal posterior insula (LdpIC) with an average gray matter thickness that was 8% less in participants with OSA than in controls (corrected p < .05; Figure 1A). By contrast, the left mid cingulate cortex (LMCC) was 20% thicker in participants with OSA than in controls (corrected p ≤ .005). No right hemispheric between-group differences were identified.

With VBM, increases in gray matter volume were identified in both thalami of those with OSA (corrected p < .05; Figure 1B). Peak locations in the right and left thalamus corresponded most closely to the ventral lateral, ventral posterior, and medial dorsal thalamic nuclei regions.

Relationship between ODI and cortical thickness

ODI data, available in 35 participants, correlated inversely with the thicknesses of both left and right dorsal posterior insular cortices (dpIC) and also with thickness of the left posterior cingulate or precuneus (Figure 2). Figure 3 demonstrates a high level of concordance between this and with the specific LdpIC region identified by the between-group comparison as being thinned in participants with OSA.

Structure and sympathetic nerve activity

In the cohort as a whole (whether quantified by CTA or by VBM), there was a significant positive correlation between MSNA BI and gray matter thickness within the left mid cingulate cortex (corrected p ≤ .05; Figure 4A). In other words, the greater the cortical thickness or gray matter volume within the left MCC, the higher was sympathetic firing incidence. With VBM, a strong positive correlation with BI was identified within a region of the left posterior thalamus corresponding to the pulvinar nucleus (corrected p ≤ .05; Figure 4B). No right hemispheric correlations with BI were identified by either method.

Discussion

The current investigation yielded three novel findings. First, comparison of autonomic network morphology of participants with and without moderate-to-severe OSA, using two distinct but complementary quantitative methods (CTA and VBM), identified in those with OSA: (1) a significantly thinner region within the left dpIC (CTA); (2) a significantly thicker region within in the left mid-cingulate (CTA); and (3) bilateral thalamic regions with greater gray matter volume (VBM). Second, there was a significant inverse relationship between the frequency of nocturnal intermittent hypoxemia (i.e., the ODI) and cortical thickness within bilateral dpIC and the left posterior cingulate or precuneus. Third, we detected significant positive correlations between muscle sympathetic BI and the thickness (CTA) or volume (VBM) of the left mid cingulate, a key component of the CAN [16], and between MSNA BI and the volume of a left posterior thalamic region corresponding to the pulvinar nucleus.

The first reported between-group comparison of cortical morphology in participants with and without moderate OSA was by Macey et al., who identified diminished gray matter in the frontal, parietal, and temporal cortices and the anterior cingulate, hippocampus, and cerebellum [24]. By contrast, O'Donoghue et al. found no significant gray matter differences

Table 1. Participant characteristics

Characteristic	All	Control (No or mild apnea)	OSA (moderate or severe apnea)	P
	n = 41	n = 19	n = 22	
Age (years)	59 ± 2	59 ± 2	59 ± 2	.999
AHI (events/hr)	20 ± 3	7 ± 1	31 ± 4	<.001
MSNA (bursts/100 HB)	63 ± 3	55 ± 4	71 ± 3	<.001
BMI (kg/m²)	29 ± 1	28 ± 1	31 ± 1	.388
HR (bpm)	60 ± 2	58 ± 2	62 ± 2	.241
SBP (mm Hg)	120 ± 2	118 ± 3	122 ± 4	.185
DBP (mm Hg)	70 ± 1	70 ± 2	70 ± 2	.905
ESS	6 ± 1	4 ± 1	7 ± 1	.547
Mean SaO$_2$ (%)	95 ± 1	95 ± 1	95 ± 1	.851
Min SaO$_2$ (%)	85 ± 1	88 ± 1	82 ± 2	.056
ODI	24 ± 4	10 ± 2	35 ± 2	<.001

Note. Values are Mean ± SE. *p*-Values relate to between-group differences. AHI = apnea–hypopnea index; bpm = beats per minute; BMI = body mass index; DBP = diastolic blood pressure; ESS = Epworth Sleepiness Scale; HB = heart beat; HR = heart rate; MSNA = muscle sympathetic nerve activity; ODI = oxygen desaturation index; SaO$_2$ = arterial oxyhemoglobin saturation; SBP = systolic blood pressure.
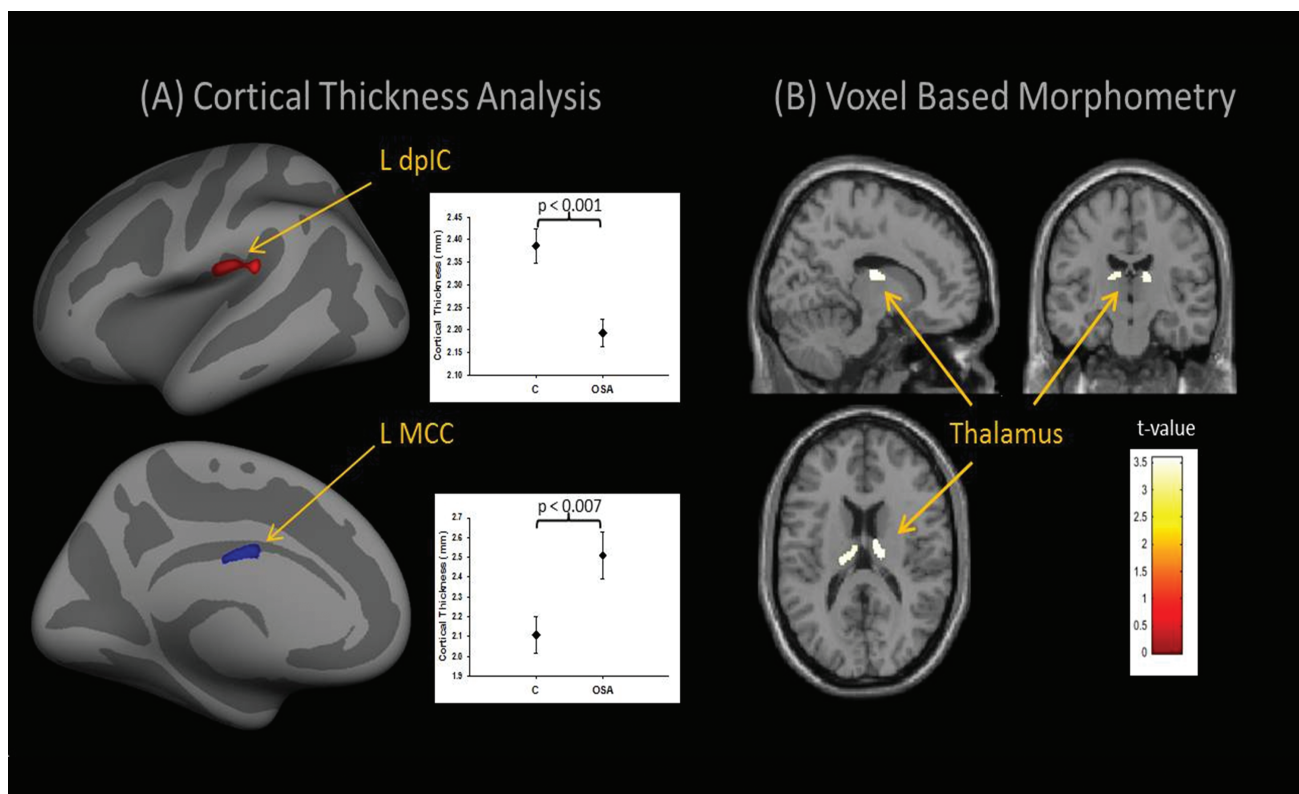
Figure 1. Group differences in gray matter. Group differences in average gray matter thickness between 19 control (C) participants with no or mild OSA and 22 participants with moderate-to-severe OSA. (A) Cortical thickness comparison of OSA to age/sex-matched C participants demonstrated, for OSA, significantly thinner LdpIC (C = 2.39 ± 0.15 mm [mean $\pm$ SD]; OSA = 2.19 ± 0.13 mm; 895 0.80 mm^2 vertices; center of gravity [CoG] $x = -47$, $y = -21$, $z = 21$; p corrected $\leq .05$) gray matter and significantly thicker LMCC (C = 2.11 ± 0.42 mm; OSA = 2.54 ± 0.54 mm; 249 0.80 mm^2 vertices; CoG $x = -5$, $y = -7$, $z = 30$; p corrected $\leq .05$) gray matter (for both, corrected $p < .05$). The inset graphs display the average cortical gray matter thickness (in mm) for both groups and both regions. (B) Voxel-based morphometry analysis revealed greater average thalamic gray matter density bilaterally in those with OSA (right COG: $x = 15$, $y = -15$, $z = 15$; 197 1.5 mm^3 voxels; left COG: $x = -17$, $y = -20$, $z = 15$; 137 1.5 mm^3 voxels; corrected $p < .05$).

between patients with an AHI >30 and control participants (AHI < 5 with airflow measured by thermistor or AHI < 15 if measured by nasal cannula) [25]. Seeking resolution, Morrell et al. combined the O'Donoghue data with those acquired at a different institution (34 participants with OSA and 35 serving as control participants). In a modified VBM analysis, reductions in gray matter were confined to the right middle temporal gyrus and bilateral cerebellum [47]. Contemporaneously, Yaouhi et al. identified, in a group of 16 participants with severe OSA, gray matter decreases in several cortical regions: the frontal and temporo–parietal–occipital cortices, thalamus, hippocampus, basal ganglia, and cerebellum [26]. Recently, Fatouleh et al. reported gray matter increases in some regions (bilateral insula, bilateral motor cortex, left hippocampus, left premotor cortex, and an extensive area encompassing the medulla/pons/cerebellum), whereas in others (right posterior cingulate, bilateral amygdala, medial prefrontal cortex, occipital lobe, and left cerebellar cortex, albeit at a lower uncorrected $p < .005$), gray matter was decreased in those with OSA [22]. All of these investigators utilized exclusively VBM. Finally, and most recently, Baril et al. reported a comparative data set demonstrating morphological changes in older participants with and without OSA using both VBM and CTA. This group correlated its physiological consequences (hypoxemia, respiratory disturbances, and sleep fragmentation) with regional increases in cortical thickness and gray matter volume, and attributed their observed changes to

local edema and reactive cellular responses caused by OSA [48]. Taken together, the inconsistency of these findings has been attributed to methodological variance, the play of chance arising from multiple comparisons of thousands of voxels and idiosyncratic application of thresholds differing in their stringency for significance [25, 47].

The present study, which applied CTA as well as VBM, focused specifically on three regions known to participate in the regulation of sympathetic outflow, blood pressure, and HR: the LdpIC, the left mid-cingulate (two key CAN nodes with afferent and efferent connections with brainstem premotor autonomic neurons that ultimately project to and control preganglionic sympathetic and parasympathetic outflow [14, 16]), and the thalamus [20–23, 49, 50]. The rationale for focusing our attention on these specific areas of interest and also in adopting stringent analytical thresholds was to diminish the probability of both false-negative and false-positive observations.

Participants with OSA exhibited both thickening and thinning of regions engaged in autonomic cardiovascular regulation. Importantly, areas that thickened demonstrated also a positive correlation with MSNA, whereas those thinned did not, suggesting differences both in the causal stimuli to such structural changes and in their functional consequences.

The precise mechanisms for such morphological variations are as yet unknown, although the inverse relationships found between the ODI and thickness of the LPCC, and both dorsal
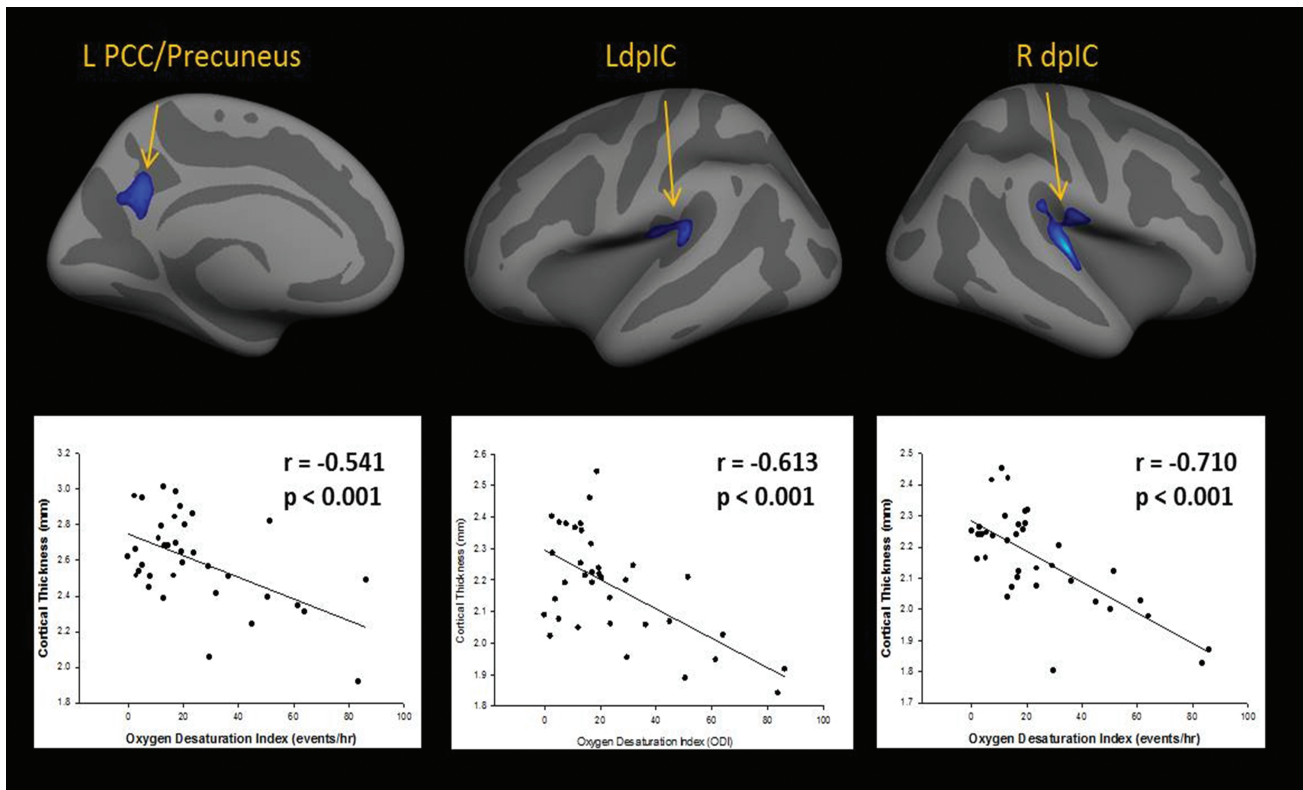
Figure 2. Gray matter correlates with oxygen desaturation index. Inverse correlations between ODI and LPCC/precuneus, LdpIC, and right dorsal posterior insula (RdpIC) gray matter thickness (*n* = 35).
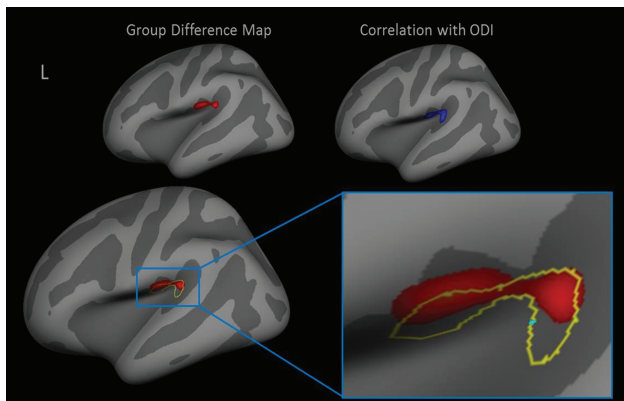

Figure 3. Overlap map: Group differences vs. correlation with ODI. Overlap map emphasizing the high correspondence, within the LdpIC, between the statistically significant (corrected *p* < .05) regions identified in the between-group comparison (mean AHI < 15 vs. AHI ≥ 15) and the correlation analysis of cortical thickness with ODI. This regional concordance is consistent with the concept that recurrent episodes of nocturnal hypoxia affect morphology. The enlarged box shows the group differences in red and the correlation with ODI outlined in yellow. ODI = oxygen desaturation index; AHI = apnea hypopnea index.

posterior insular cortices suggest a selective susceptibility of these specific cortical autonomic regions to hypoxic damage. Over months and years, recurring cycles of apnea and hypopnea accompanied by intermittent hypoxia and reoxygenation could promote cell death directly via hypoxia [51, 52] or indirectly by generating free radical species, thus thinning vulnerable brain areas [53]. In a study by Metz et al., functional gray matter reductions within the medial prefrontal cortex of rats following spared nerve injury were attributed to increased N-methyl-d-aspartate receptor currents in basal dendritic spines, facilitating calcium mediated excito-toxicity and neuronal loss [54].

A second plausible cause of either thinning or thickening of gray matter may be changes in sensory input to cortical autonomic regions, resulting in altered cellular utilization. Consequent adaptations in glial and/or neuronal cell size and changes in axonal architecture, by apoptosis, synaptogenesis, and/or dendritic re-organization would be appreciated by imaging studies as differences in gray matter volume, density, or thickness [55–57]. For example, persistent sensorimotor impairment after surgical repair of complete median nerve transection is associated with loss of contra-lesion somatosensory cortex gray matter [44]. Conversely, 8 consecutive days of painful stimulation increased the gray matter of pain-related brain areas [58]. The frequency of arousal from sleep, independently of apnea, is also a strong correlate of sympathetic nerve firing during wakefulness [12]. One structural change associated with disruption of neurocellular circadian metabolic rhythms by chronic sleep fragmentation is hippocampal subfield atrophy [59].

The posterior insula, or primary interoceptive cortex [60], possesses a direct reciprocal pathway with the nucleus of the solitary tract (NTS) and a secondary pathway from the NTS through the parabrachial nucleus [61, 62]. An indirect efferent pathway, via the lateral hypothalamus, links the posterior insula and the rostral ventral lateral medulla, the brainstem origin of most premotor sympathetic outflow [63]. In humans, electrical stimulation of the left insular cortex causes, in general,
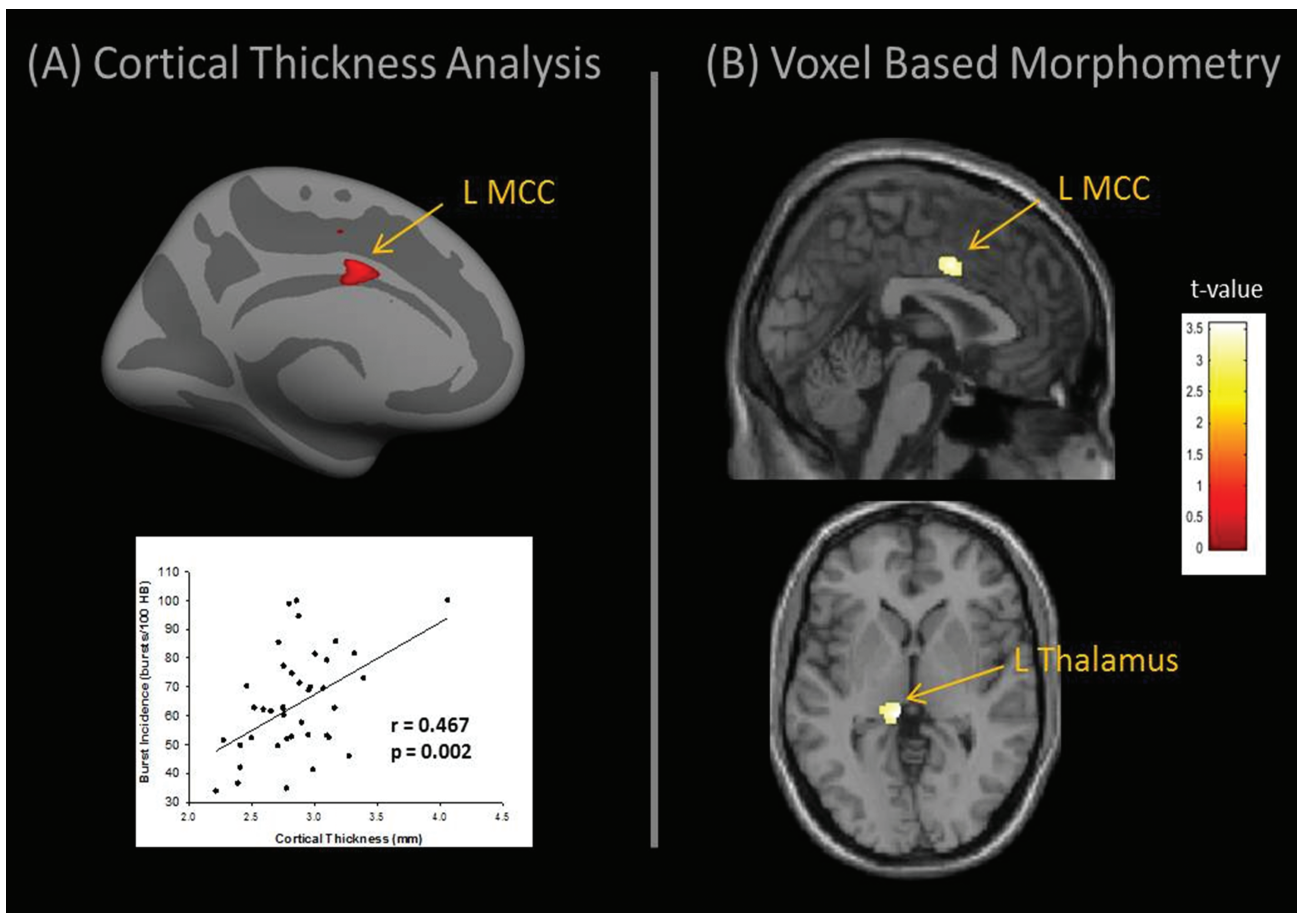
Figure 4. Gray matter correlates with burst incidence. (A) Cortical thickness within the LMCC (COG $x = -5$, $y = 0$, $z = 31$; 367 vertices) correlates significantly with resting burst incidence across all participants ($r = 0.467$; $p = .002$). (B) Voxel-based morphometry revealed that gray matter density within the LMCC also correlated with burst incidence (COG $x = -1$, $y = 2$, $z = 38$; corrected $p < .05$). Furthermore, a region in the left posterior thalamus ($x = -8$, $y = -32$, $z = 0$) also correlated positively with gray matter density.

bradycardia and a fall in blood pressure, whereas right-sided stimulation elicits the opposite response [64].

In the present series, the ODI, a measure of the severity of OSA-induced hypoxemia, related significantly and inversely to cortical thickness within the LdpIC, the right dorsal posterior insula, and the left posterior cingulate or precuneus. Of these three areas, only the LdpIC, i.e., the vasodepressor region, emerged as a region thinned significantly in OSA (Figure 3). Thus, one mechanism contributing to central upward resetting of noradrenergic traffic in OSA could be loss of the normal restraint exerted on sympathetic outflow and the baroreceptor reflex by certain cortical SN elements, such as the left posterior insula [64], that may be particularly susceptible to hypoxia and reperfusion-mediated cell damage. However, no significant correlation between MSNA BI and cortical thickness was identified for either the LdpIC or for either of the other two specific regions of thinning. Fatouleh et al, concluded, from their own MRI observations, "that asphyxic damage due to repeated episodes of nocturnal apnoea is not the main cause of the sympathoexcitation" of OSA [22].

Conversely, these CTA and VBM analyses identified two such autonomic regions that were both significantly thickened in participants with OSA relative to controls and for which thickness or volume correlated significantly with sympathetic BI: the left

mid cingulate cortex, which receives input from a diverse array of thalamic nuclei [65, 66], and a region of the left posterior thalamus (Figure 4). The present observations argue for an important structural and functional contribution of both regions to the chronic sympathetic excitation of OSA.

How might these changes be effected? Analogous to sensory input, repeated exposure to stimuli eliciting acute autonomic responses can also induce molecular adaptations, including sustained up-regulation of components of the brain renin–angiotensin–aldosterone system. One consequence is amplification of blood pressure responses to subsequent challenges [67]. The trophic and apoptotic properties of the cortical neuronal sympathetic neurotransmitter, norepinephrine [68], have similar neuroplastic potential.

In this context, the feature of moderate-to-severe OSA most likely to induce both cortical thickening and autonomic neuroplasticity is sensitization of the peripheral chemoreceptor reflex, by repeated exposure to nocturnal hypoxemia and reperfusion. Sensitization augments the noradrenergic, hemodynamic, and ventilatory responses to hypoxia [69, 70] through mechanisms involving central angiotensin II up-regulation [71]. Peripheral chemoreceptive information travels to the brainstem and cortex via small-diameter glossopharyngeal (IX) and vagal (X) nerve fibres and from peripheral lamina I neurons of the spinal cord

ascending through the spinothalamic and spinoreticular tracts [60, 72, 73]. Cranial nerves IX and X terminate primarily in the medullary NTS, a region that receives collaterals from lamina 1 neurons [60, 72, 73]. Both NTS and lamina I afferents relay through the parabrachial nucleus and synapse within the posterior ventral medial, ventral medial, and ventral caudal portions of the medial dorsal thalamic nucleus [60, 73]. The latter then projects to the mid cingulate [74]. Homeostatic information (including that concerning stimuli that elevate blood pressure and HR) also projects to the posterior insula [60, 73]. Thus, there are established pathways by which chronically augmented chemoreceptor input could induce the cingulate and thalamic thickening and correlations with central sympathetic outflow observed in the present participants with moderate-to-severe OSA.

This study has several important strengths that merit emphasis. First, because our population is comprised primarily of middle-aged and older participants, our findings are more relevant to the population at cardiovascular risk than are observations in young adults. Second, because of the high prevalence of asymptomatic and undiagnosed OSA in the general population, all participants, including self-reported healthy controls, underwent overnight polysomnography. In five of our self-reported healthy participants, polysomnography identified previously unrecognized moderate-to-severe OSA, and 12 self-reported healthy control participants were diagnosed with mild OSA (AHI > 5 but <15). It has been a common practice to label volunteers as healthy controls if they report no nighttime snoring or daytime sleepiness. The present study avoids the selection bias that risks aggregation of disproportionate sleepy or obese individuals as an OSA cohort and calls into question the conclusions of prior studies in middle-aged participants reliant on symptoms of daytime sleepiness triggering referral for further investigation or on self-reported normal sleep for dichotomization into OSA and non-OSA cohorts.

Although MSNA and MRI data were acquired on separate experimental days, a considerable body of evidence confirms the reproducibility of resting MSNA [38] and MSNA responses to a variety of challenges (i.e., head-up tilt, lower body negative pressure, and cold pressor) when repeated following short time intervals [75, 76]. Furthermore, to minimize variation, participant preparation was identical prior to MRI and MSNA. Our interpretation is that the identified cortical differences between groups occur secondary to OSA. However, although remote, we cannot exclude the possibility that such changes may be involved in the pathogenesis of OSA.

There is accumulating evidence that acute sympathoexcitatory stimuli can induce persistent changes in the central nervous system that alter blood pressure and HR regulation [67]. Because of its severity, OSA could be considered a challenge to homeostasis with the high probability of inducing neuroplastic changes within autonomic regulatory regions. As confirmation, in the present cohort with OSA, we identified qualitatively distinct and site-specific changes in the morphology of cortical regions participating in autonomic regulation in conjunction with increased efferent sympathetic discharge during wakefulness. We conclude that the magnitude of insular thinning, although a function of hypoxia severity, does not influence MSNA, whereas cingulate and thalamic thickening relate directly to the intensity of sympathetic discharge during wakefulness.

References

1. Malpas SC. Sympathetic nervous system overactivity and its role in the development of cardiovascular disease. *Physiol Rev* 2010; **90**:513–557.
2. Floras JS, *et al*. The sympathetic/parasympathetic imbalance in heart failure with reduced ejection fraction. *Eur Heart J* 2015; **36**:1974–182b.
3. Esler M. The 2009 Carl Ludwig Lecture: Pathophysiology of the human sympathetic nervous system in cardiovascular diseases: the transition from mechanisms to medical management. *J Appl Physiol (1985)* 2010; **108**:227–237.
4. Esler M, *et al*. Sympathetic nervous system and insulin resistance: from obesity to diabetes. *Am J Hypertens* 2001; **14**:304S–309S.
5. Grassi G, *et al*. The sympathetic nervous system alterations in human hypertension. *Circ Res* 2015; **116**:976–990.
6. Shen MJ, *et al*. Role of the autonomic nervous system in modulating cardiac arrhythmias. *Circ Res* 2014; **114**:1004–1021.
7. Bradley TD, *et al*. Obstructive sleep apnoea and its cardiovascular consequences. *Lancet* 2009; **373**:82–93.
8. Floras JS. Sympathetic nervous system in patients with sleep related breathing disorders. *Curr Hypertens Rev* 2016; **12**:18–26.
9. Carlson JT, *et al*. Augmented resting sympathetic activity in awake patients with obstructive sleep apnea. *Chest* 1993; **103**:1763–1768.
10. Spaak J, *et al*. Muscle sympathetic nerve activity during wakefulness in heart failure patients with and without sleep apnea. *Hypertension* 2005; **46**:1327–1332.
11. Abboud F, *et al*. Obstructive sleep apnea and insight into mechanisms of sympathetic overactivity. *J Clin Invest* 2014; **124**:1454–1457.
12. Taylor KS, *et al*. Arousal from sleep and sympathetic excitation during wakefulness. *Hypertension* 2016; **68**:1467–1474.

13. Taylor KS, *et al.* Association between resting-state brain functional connectivity and muscle sympathetic burst incidence. *J Neurophysiol* 2016; **115**:662–673.

14. Cechetto DF, *et al.* Functional neuroanatomy of autonomic regulation. *Neuroimage* 2009; **47**:795–803.

15. Gianaros PJ, *et al.* A review of neuroimaging studies of stressor-evoked blood pressure reactivity: emerging evidence for a brain-body pathway to coronary heart disease risk. *Neuroimage* 2009; **47**:922–936.

16. Thayer JF, *et al.* A model of neurovisceral integration in emotion regulation and dysregulation. *J Affect Disord* 2000; **61**:201–216.

17. Henderson LA, *et al.* Brain responses associated with the Valsalva maneuver revealed by functional magnetic resonance imaging. *J Neurophysiol* 2002; **88**:3477–3486.

18. Kimmerly DS, *et al.* Cortical regions associated with autonomic cardiovascular regulation during lower body negative pressure in humans. *J Physiol* 2005; **569**:331–345.

19. Harper RM, *et al.* fMRI responses to cold pressor challenges in control and obstructive sleep apnea subjects. *J Appl Physiol (1985)* 2003; **94**:1583–1595.

20. Macefield VG, *et al.* Neural sites involved in the sustained increase in muscle sympathetic nerve activity induced by inspiratory capacity apnea: a fMRI study. *J Appl Physiol (1985)* 2006; **100**:266–273.

21. Kimmerly DS, *et al.* Apnea-induced cortical BOLD-fMRI and peripheral sympathoneural firing response patterns of awake healthy humans. *PLoS One* 2013; **8**:e82525.

22. Fatouleh RH, *et al.* Functional and structural changes in the brain associated with the increase in muscle sympathetic nerve activity in obstructive sleep apnoea. *Neuroimage Clin* 2014; **6**:275–283.

23. James C, *et al.* Real-time imaging of cortical and subcortical control of muscle sympathetic nerve activity in awake human subjects. *Neuroimage* 2013; **70**:59–65.

24. Macey PM, *et al.* Brain morphology associated with obstructive sleep apnea. *Am J Respir Crit Care Med* 2002; **166**:1382–1387.

25. O'Donoghue FJ, *et al.* Cerebral structural changes in severe obstructive sleep apnea. *Am J Respir Crit Care Med* 2005; **171**:1185–1190.

26. Yaouhi K, *et al.* A combined neuropsychological and brain imaging study of obstructive sleep apnea. *J Sleep Res* 2009; **18**:36–48.

27. Canessa N, *et al.* Obstructive sleep apnea: brain structural changes and neurocognitive function before and after treatment. *Am J Respir Crit Care Med* 2011; **183**:1419–1426.

28. Bookstein FL. "Voxel-based morphometry" should not be used with imperfectly registered images. *Neuroimage* 2001; **14**:1454–1462.

29. Davatzikos C. Why voxel-based morphometric analysis should be used with great caution when characterizing group differences. *Neuroimage* 2004; **23**:17–20.

30. Kasai T, *et al.* Sleep apnea and cardiovascular disease: a bidirectional relationship. *Circulation* 2012; **126**:1495–1510.

31. Franklin KA, *et al.* Obstructive sleep apnea is a common disorder in the population-a review on the epidemiology of sleep apnea. *J Thorac Dis* 2015; **7**:1311–1322.

32. Johns MW. Sleepiness in different situations measured by the Epworth Sleepiness Scale. *Sleep* 1994; **17**:703–710.

33. Rechtschaffen A, *et al.* *A Manual of Standardized Terminology, Techniques and Scoring System for Sleep Stages of Human Subjects.* Los Angeles: UCLA Brain Information Service/Brain Research Institute; 1968.

34. Sleep Disorders Atlas Task Force. EEG arousals: scoring rules and examples: a preliminary report from the Sleep Disorders Atlas Task Force of the American Sleep Disorders Association. *Sleep* 1992; **15**:173–184.

35. American Academy of Sleep Medicine Task Force. Sleep-related breathing disorders in adults: reccomendations for syndrome definition and measurement techniques in clinical research. The report of an American Academy of Sleep Medicine Task Force. *Sleep* 1999; **22**:667–689.

36. Iber C, *et al.* *The AASM Manual for the Scoring of Sleep and Associated Events: Rules, Terminology, and Technical Specifications.* Westchester, IL: The American Academy of Sleep Medicine; 2007.

37. Floras JS, *et al.* Inhibition of muscle sympathetic nerve activity in humans by arginine vasopressin. *Hypertension* 1987; **10**:409–416.

38. Floras JS, *et al.* Sympathoneural and haemodynamic characteristics of young subjects with mild essential hypertension. *J Hypertens* 1993; **11**:647–655.

39. Dale AM, *et al.* Cortical surface-based analysis. I. Segmentation and surface reconstruction. *Neuroimage* 1999; **9**:179–194.

40. Fischl B, *et al.* Cortical surface-based analysis. II: Inflation, flattening, and a surface-based coordinate system. *Neuroimage* 1999; **9**:195–207.

41. Fischl B, *et al.* High-resolution intersubject averaging and a coordinate system for the cortical surface. *Hum Brain Mapp* 1999; **8**:272–284.

42. Fischl B, *et al.* Measuring the thickness of the human cerebral cortex from magnetic resonance images. *Proc Natl Acad Sci U S A* 2000; **97**:11050–11055.

43. Talairach J, *et al.* *Co-planar Stereotaxic Atlas of the Human Brain.* New York: Thieme Medical Publishers Inc.; 1988.

44. Taylor KS, *et al.* Cutting your nerve changes your brain. *Brain* 2009; **132**:3122–3133.

45. Ashburner J, *et al.* Voxel-based morphometry–the methods. *Neuroimage* 2000; **11**(6 Pt 1):805–821.

46. Ashburner J. A fast diffeomorphic image registration algorithm. *Neuroimage* 2007; **38**:95–113.

47. Morrell MJ, *et al.* Changes in brain morphology in patients with obstructive sleep apnoea. *Thorax* 2010; **65**:908–914.

48. Baril AA, *et al.* Gray matter hypertrophy and thickening with obstructive sleep apnea in middle-aged and older adults. *Am J Respir Crit Care Med* 2017; **195**:1509–1518.

49. Harper RM, *et al.* Lateralized and widespread brain activation during transient blood pressure elevation revealed by magnetic resonance imaging. *J Comp Neurol* 2000; **417**:195–204.

50. Beissner F, *et al.* The autonomic brain: an activation likelihood estimation meta-analysis for central processing of autonomic function. *J Neurosci* 2013; **33**:10503–10511.

51. Gozal D. CrossTalk proposal: the intermittent hypoxia attending severe obstructive sleep apnoea does lead to alterations in brain structure and function. *J Physiol* 2013; **591**:379–381.

52. Rosenzweig I, *et al.* Sleep apnoea and the brain: a complex relationship. *Lancet Respir Med* 2015; **3**:404–414.

53. Lavie L. Oxidative stress in obstructive sleep apnea and intermittent hypoxia–revisited–the bad ugly and good: implications to the heart and brain. *Sleep Med Rev* 2015; **20**:27–45.

54. Metz AE, *et al.* Morphological and functional reorganization of rat medial prefrontal cortex in neuropathic pain. *Proc Natl Acad Sci U S A* 2009; **106**:2423–2428.

55. Blankstein U, *et al*. The complex minds of teenagers: neuroanatomy of personality differs between sexes. *Neuropsychologia* 2009; **47**:599–603.

56. May A, *et al*. Structural brain alterations following 5 days of intervention: dynamic aspects of neuroplasticity. *Cereb Cortex* 2007; **17**:205–210.

57. May A. Chronic pain may change the structure of the brain. *Pain* 2008; **137**:7–15.

58. Teutsch S, *et al*. Changes in brain gray matter due to repetitive painful stimulation. *Neuroimage* 2008; **42**:845–849.

59. Joo EY, *et al*. Hippocampal substructural vulnerability to sleep disturbance and cognitive impairment in patients with chronic primary insomnia: magnetic resonance imaging morphometry. *Sleep* 2014; **37**:1189–1198.

60. Craig AD. How do you feel? Interoception: the sense of the physiological condition of the body. *Nat Rev Neurosci* 2002; **3**:655–666.

61. Verberne AJM. Modulation of autonomic function by the cerebral cortex. In: Llewellyn-Smith IJ, Vernerne AJM, eds. *Central Regulation of Autonomic Functions*. 2nd ed. New York: Oxford University Press, Inc., 2011: 202–219.

62. Andresen MC, *et al*. The nucleus of the solitary tract: processing information from viscerosensory afferents. In: Llewellyn-Smith IJ, Verberne AJM, eds. *Central Regulation of Autonomic Functions*. 2nd ed. New York: Oxford University Press, Inc.; 2013:23–46.

63. Sun MK, *et al*. Hypothalamic glutamatergic input to medullary sympathoexcitatory neurons in rats. *Am J Physiol* 1986; **251**:R798–R810.

64. Oppenheimer SM, *et al*. Cardiovascular effects of human insular cortex stimulation. *Neurology* 1992; **42**:1727–1732.

65. Devinsky O, *et al*. Contributions of anterior cingulate cortex to behaviour. *Brain* 1995; **118**:279–306.

66. Hatanaka N, *et al*. Thalamocortical and intracortical connections of monkey cingulate motor areas. *J Comp Neurol* 2003; **462**:121–138.

67. Johnson AK, *et al*. The roles of sensitization and neuroplasticity in the long-term regulation of blood pressure and hypertension. *Am J Physiol Regul Integr Comp Physiol* 2015; **309**:R1309–R1325.

68. Mitchell DA, *et al*. Jugular venous overflow of noradrenaline from the brain: a neurochemical indicator of cerebrovascular sympathetic nerve activity in humans. *J Physiol* 2009; **587**:2589–2597.

69. Narkiewicz K, *et al*. Selective potentiation of peripheral chemoreflex sensitivity in obstructive sleep apnea. *Circulation* 1999; **99**:1183–1189.

70. Dempsey JA, *et al*. Pathophysiology of sleep apnea. *Physiol Rev* 2010; **90**:47–112.

71. Weiss JW, *et al*. Sympathoexcitation and arterial hypertension associated with obstructive sleep apnea and cyclic intermittent hypoxia. *J Appl Physiol (1985)* 2015; **119**:1449–1454.

72. Kvetnansky R, *et al*. Catecholaminergic systems in stress: structural and molecular genetic approaches. *Physiol Rev* 2009; **89**:535–606.

73. Saper CB. The central autonomic nervous system: conscious visceral perception and autonomic pattern generation. *Annu Rev Neurosci* 2002; **25**:433–469.

74. Vogt BA, *et al*. Cingulate cortex of the rhesus monkey: I. Cytoarchitecture and thalamic afferents. *J Comp Neurol* 1987; **262**:256–270.

75. Kimmerly DS, *et al*. Test-retest repeatability of muscle sympathetic nerve activity: influence of data analysis and head-up tilt. *Auton Neurosci* 2004; **114**:61–71.

76. Schobel HP, *et al*. Influence of resting sympathetic activity on reflex sympathetic responses in normal man. *Clin Auton Res* 1995; **5**:71–80.